REVIEW

Research Progress in Cucurbit[*n*]uril-Based Metal Nanomaterials for Electrocatalytic Applications

Zong-Nan Wei [a,b], Min-Na Cao [b,*], Rong Cao [b,*]

[a] Department of Chemistry, University of Science and Technology of China, Hefei, Anhui 230026, China
[b] State Key Laboratory of Structural Chemistry, Fujian Institute of Research on the Structure of Matter, Chinese Academy of Sciences, Fuzhou 350002, China

Abstract

Metal nanomaterials have exhibited excellent performance in electrocatalytic applications, but they still face the problems of poor stability and limited regulation strategies. It is an efficient strategy for greatly enhanced catalytic activity and stability by introducing a second component. In this review, we provide the sketch for the combination of metal nanomaterials and cucurbit[*n*]urils (CB[*n*]s) in electrocatalytic applications. CB[*n*]s are a series of macrocycles with rigid structure, high stability, and function groups for coordinating with metal sites, which make them promising to stabilize and modulate the metal nanomaterials for ideal performance. The discussion classifies the roles of CB[*n*]s, involving CB[*n*]s as protecting agents, CB[*n*]-based supramolecular self-assemblies and CB[*n*]s as the precursor for the preparation of N-doped holy carbon matrix. Various metal nanocatalysts including metal (Pt, Ir, Pd, Ru, Au) nanoparticles, metal (Fe, Co, Ni) single-atoms, and transition metal carbides (TMCs) have been integrated with CB[*n*] or CB[*n*]-derived carbon matrix. These nanomaterials show superior activity and stability in multiple electrocatalytic reactions, including oxygen reduction reaction (ORR), oxygen evolution reaction (OER), hydrogen evolution reaction (HER), carbon dioxide reduction reaction (CO_2RR), methanol oxidation reaction (MOR), and ethanol oxidation reaction (EOR). Furthermore, a few metal-CB[*n*] composites can become bifunctional catalysts applied in the overall water splitting and fuel cell. It is surprising that the activity of CB[*n*]-based nanocatalysts is comparable with that of commercial catalyst, and the stability is even better. The experimental analysis together with the density functional theory (DFT) calculations verifies that the improvement can be attributed to the interaction between the metal nanocrystal and CB[*n*]s as well as the characteristic stability of CB[*n*]s. Finally, we talk about the challenges and opportunities for the cucurbit[*n*]uril-based electrocatalysis. This review provides an impressive strategy to obtain well-defined metal nanomaterials constructed with CB[*n*]s with enhanced performance, and expects that such a strategy will develop more efficient catalysts for a broader range of electro-applications.

Keywords: Electrocatalysis; Fuel cells; Water splitting; cucurbit[*n*]uril; Metal nanomaterials

1. Introduction

Electrocatalysis is a process in which a catalyst can accelerate a redox reaction on the surface of an electrode under applied potentials. Efficient electrocatalysis using renewable electricity can offer a promising energy conversion strategy to afford high-valuable feedstocks, which is expected to facilitate carbon neutrality [1,2]. Hence, developing high-efficiency electrocatalysts is urgently needed. Currently, electrocatalysts have been widely applied in fuel cells to promote the cathodic oxygen reduction reaction (ORR), such as the direct methanol fuel cells (DMFCs) and the direct ethanol fuel cells (DEFCs), water splitting composed of the hydrogen evolution reaction (HER) and the oxygen evolution reaction (OER), and the carbon dioxide reduction reaction (CO_2RR). In all these applications, the reactions always trouble with some similar problems, for example, the sluggish thermodynamics and kinetics, together with the highly corrosive reaction intermediate, which greatly restrict the efficiency [3−6]. Moreover, commercial catalysts, like Pt/C and Pd/C, have a high cost and face quick deactivation arising from the metal particles aggregation and the carbon support

Received 15 July 2022; revised 17 August 2022; Accepted 1 September 2022; Available online 4 September 2022

* Corresponding author, Rong Cao, Tel: (86-591)83714517, E-mail address: rcao@fjirsm.ac.cn.
* Corresponding author, Min-Na Cao, Tel: (86-591)83714517, E-mail address: mncao@fjirsm.ac.cn.

https://doi.org/10.13208/j.electrochem.2215008

corrosion, causing failure to fulfill practical applications [7,8]. Accordingly, it is highly desired to explore efficient and cost-effective electrocatalysts with enhanced catalytic activity and excellent durability.

Metal nanomaterials have been widely studied for electrocatalysis with unique crystal structures, well-defined facets, and high surface area [9,10]. For example, Cu nanocubes (NCs) with the size of 44 nm exhibited the enhanced selectivity of CO_2RR with the faradaic efficiency (FE) of 80% at −1.1 V *vs.* reversible hydrogen electrode (RHE), suggesting a 1.43-fold enhancement compared with the common Cu foil [11]. However, metal nanomaterials are usually plagued by agglomeration and decrease of surface area, leading to poor stability and reduced activity. It has been reported that the degradation of the Cu NCs turned more serious with a smaller size, and caused an obvious decrease of the FE toward CO_2RR and an increase of the FE toward competitive HER [12].

Introducing a second component into metal nanomaterial is an effective strategy to enhance the activity and stability of the catalysts [13]. Moreover, the interaction between the nanosized metal and the second component might modulate the electronic properties of the active sites [2]. In one study, well-dispersed Ru nanoparticles were supported on a nitrogenated holey two-dimensional carbon structure ($Ru@C_2N$) [14]. For HER, the $Ru@C_2N$ catalyst showed low overpotentials at 10 $mA \cdot cm^{-2}$ (13.5 mV in 0.5 $mol \cdot L^{-1}$ H_2SO_4 and 17.0 mV in 1.0 $mol \cdot L^{-1}$ KOH), and high stability in 10,000 potential cycles. Such performance was comparable with the commercial Pt/C, due to the similar hydrogen binding energy, which is demonstrated by the density functional theory (DFT) calculations. In another study, novel core-shell structured nanoparticles with Au core and $AuIr_2$ alloy shell ($Au@AuIr_2$) were employed as an efficient catalyst for the overall water splitting (Fig. 1) [15]. The interaction between Au and Ir atoms could construct partially oxidized surfaces and thus enhance their catalytic activity by 4.6 times toward OER compared with those of commercial Ir catalysts. Moreover, this catalyst showed excellent HER catalytic properties comparable to those of commercial Pt/C. Then, the $Au@AuIr_2$ catalyst used in the overall water splitting cell achieved an outstanding activity for a low cell voltage of 1.55 V at 10 $mA \cdot cm^{-2}$ and stability for more than 40 h, while for commercial Ir/C||Pt/C, the low cell voltage was 1.63 V maintained within few minutes. Both the experimental results and the DFT calculations revealed that the distinctive partially oxidized surfaces could balance different

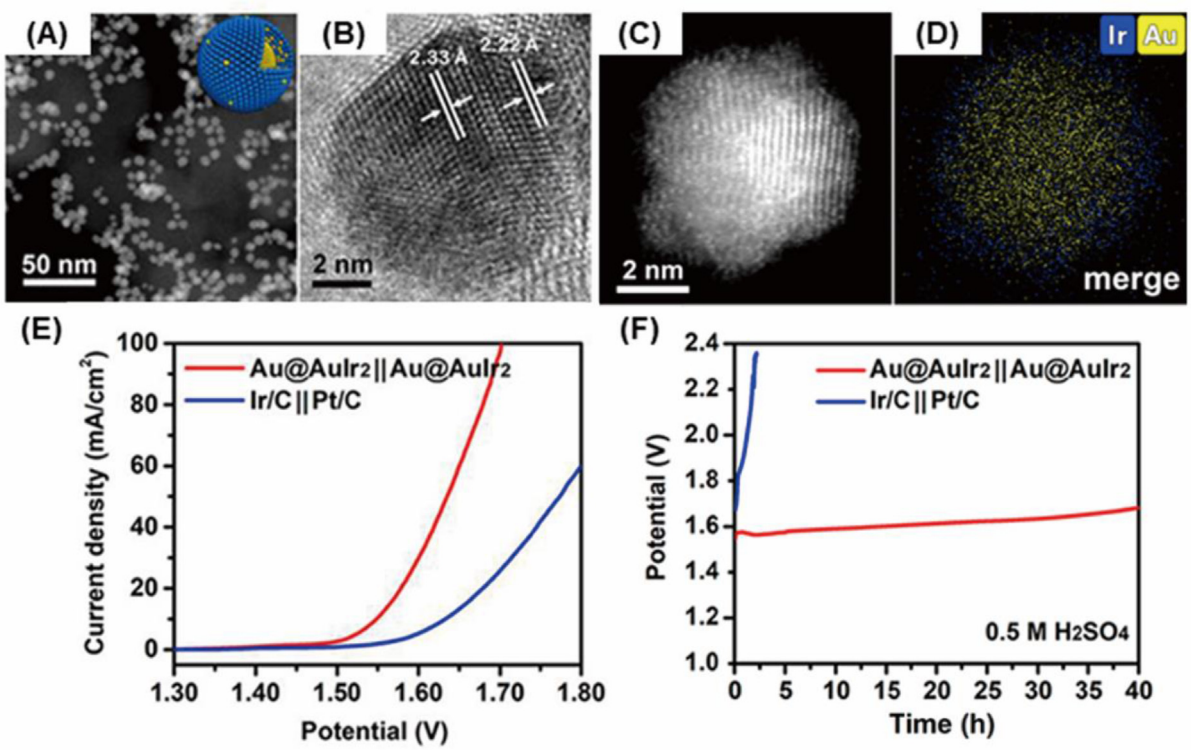

Fig. 1. (A) Low-magnification dark-field and (B) high-resolution transmission electron microscopic (TEM) images of $Au@AuIr_2$. (C) High-angle annular darkfield scanning TEM image and the corresponding energy dispersive X-ray (EDX) mapping of (D) merged signal of Au (gold), and Ir (blue). (E) Polarization and (F) chronopotentiometric curves at 10 $mA \cdot cm^{-2}$ for overall water splitting of $Au@AuIr_2||Au@AuIr_2$ and Ir/C||Pt/C. Reproduced with permission of Ref [15]. Copyright 2021, American Chemical Society.

binding intermediates to enhance the performance. From the above reports, it can be seen that introducing a second component will greatly regulate the metal electronic properties, and enhance the activity and stability.

Cucurbit[*n*]urils (CB[*n*]s, $n = 5-8,10,14$) are a series of rigid macrocycles constructed by glycoluril units and methylene bridges with a hollowed-out pumpkin shape and a hydrophobic cavity (Fig. 2) [16]. CB[*n*]s were first obtained by Behrend and coworkers in 1905 through an acid-catalyzed condensation reaction of glycoluril and formaldehyde, and the chemical structure characterization of CB[*n*]s was uncovered by Mock and co-workers in 1981 [17,18]. For Cucurbit[*n*]urils, *n* is the number of monomers. With the increased *n* value, the size of the hollow cavity enlarges. When the cavity is large enough, CB[*n*]s, as host molecules, can partially or even completely envelop some guest molecules in the cavity to form an inclusion [19]. Moreover, the charge on the surface of cucurbit[*n*]uril has a special distribution, especially the negative carbonyl-fringed portals that have strong interaction with positively charged guests. In addition, cucurbit[*n*]urils exhibit high chemical and thermal stabilities. The most stable macrocyclic CB[*n*] is CB[6], composed of six glycoluril units and twelve methylene bridges. However, CB[*n*]s have poor solubility in water and organic solvents, which limits their development. For example, CB[*n*]s with poor solubility would be hard to bind with metal and organic ions in the neutral condition, causing trouble with supramolecular self-assembly formation [20]. To solve such problems, decamethylcucurbit[5]uril (Me_{10}CB[5]) was firstly synthesized by fully methyl-substituted glycolurils instead of glycolurils as the precursor and showed enhanced solubility in water.

Because of their excellent stability, hydrophobic cavities for guest molecules, function groups at the end position for coordination, and rich surface charge, CB[*n*]s are very suitable to be combined with metal nanomaterial, and shed influence on their activity and stability. For the first time, gold nanoparticles (Au NPs) capped by CB[5] (CB[5]-AuNP) were obtained, where CB[5] played the role in the limitation of growth or merging of AuNPs [22]. The composites showed enhanced stability, due to the strong interaction between the Au NPs and CB[5] via their electron-rich carbonyl portals. Moreover, the self-assembly of the CB[*n*] with the metal ion is another effective strategy for the well-defined nanocrystal superstructures [23]. Our group verified the vital role of CB[*n*]s in the nanocrystal application in the Suzuki-Miyaura cross-coupling reactions and Heck cross-coupling reactions. In one work, palladium nanoparticles (Pd NPs) with different shapes and sizes protected by CB[6] (CB[6]-Pd NPs) were obtained [24]. Additionally, CB[6]-Pd NPs showed excellent catalytic performance for direct C-H functionalization reaction [25]. The catalyst exhibited excellent performance and remarkable stability due to the electrostatic interaction between CB[6] and Pd NPs. In another example, a series of supramolecular assemblies ($MPdMe_{10}$CB[5], M = Li, Na, K, Rb, or Cs) were obtained and used as efficient catalysts for Heck cross-coupling reactions [26]. The authors uncovered the vital role of Me_{10}CB[5] to control the release of active Pd species from the crystalline hybrid catalysts into the reaction system to ensure good recyclability.

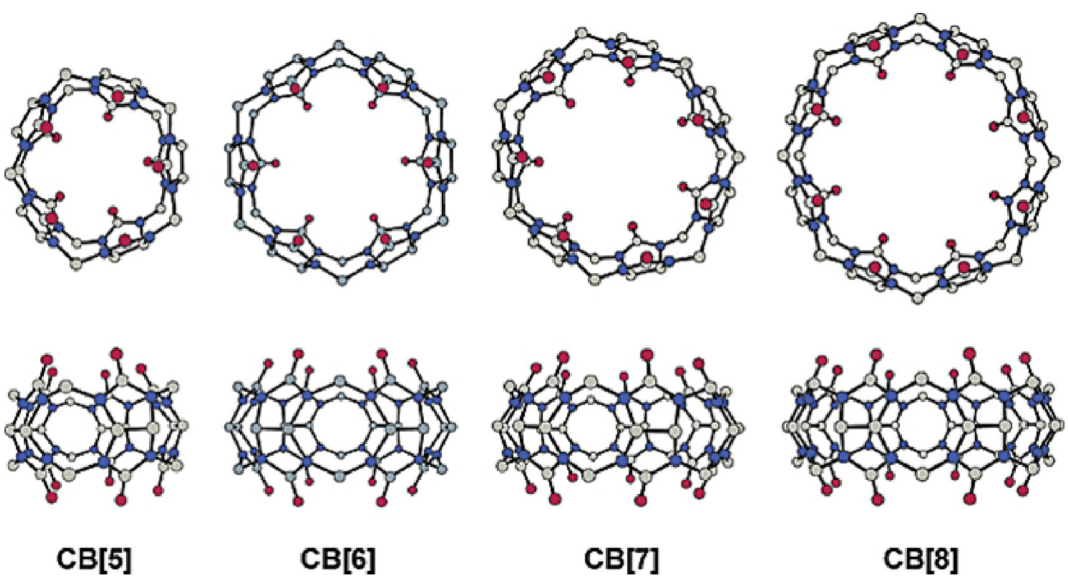

Fig. 2. X-ray crystal structures of CB[n] (n = 5–8). Color codes: carbon, gray; nitrogen, blue; oxygen, red. Reproduced with permission of Ref [21]. Copyright 2003, American Chemical Society.

Combined with the favorable property of nanomaterials and the remarkable stability of CB[*n*]s, the metal-CB[*n*] composites showed an excellent performance in organic catalysis, which inspires us to extend their application to electrocatalysis. In recent years, our group has made considerable efforts in developing the metal NPs constructed with the CB[*n*]s and obtained considerable achievements. In this review, we will summarize the role of CB[*n*]s in electrocatalysis in the following three aspects (Fig. 3). (i) CB[*n*]s as the protecting agents to restrict the growth of metal crystals. (ii) CB[*n*] as the host molecules to construct the supramolecular self-assemblies. (iii) CB[*n*]s as the precursors for N-doped carbon matrix via pyrolysis. In the end, we offer a summary together with perspectives on the challenges and opportunities for cucurbit[*n*]uril-based metal nanomaterials applied for electrocatalysis.

2. Cucurbit[*n*]urils as protecting agents

For the huge cucurbit[*n*]uril family, Cucurbit[6]uril (CB[6]) stands out with a lot of advantages. CB[6] is composed of six glycoluril units fused by twelve methylene. CB[6] has interactions with metal nanoparticles (NPs) through electrostatic attraction between its carboxylate portals and the surface atoms of NPs. Importantly, CB[6] as a rigid macrocyclic molecule when capping on the metal NPs can leave enough accessible active sites on the surface for substrates sorption during the catalytic procedure. Taking these advantages, our group has successfully prepared a series of CB[6]-metal nanocomposites as electrocatalysts for energy conversions.

Electrolytic water splitting is the most promising method for large-scale hydrogen production. For the anodic half-reaction of water splitting, the 4-electron-transfer oxygen evolution reaction (OER) has been plagued by sluggish reaction kinetics, especially in acidic media required for higher overpotential causing serious catalyst degradation. For the complicated OER, effective and long-life catalysts are prerequisites to minimizing overpotential to realize commercial large-scale production. Ir-based materials are the most suitable electrocatalysts for OER in acidic electrolytes [27,28].

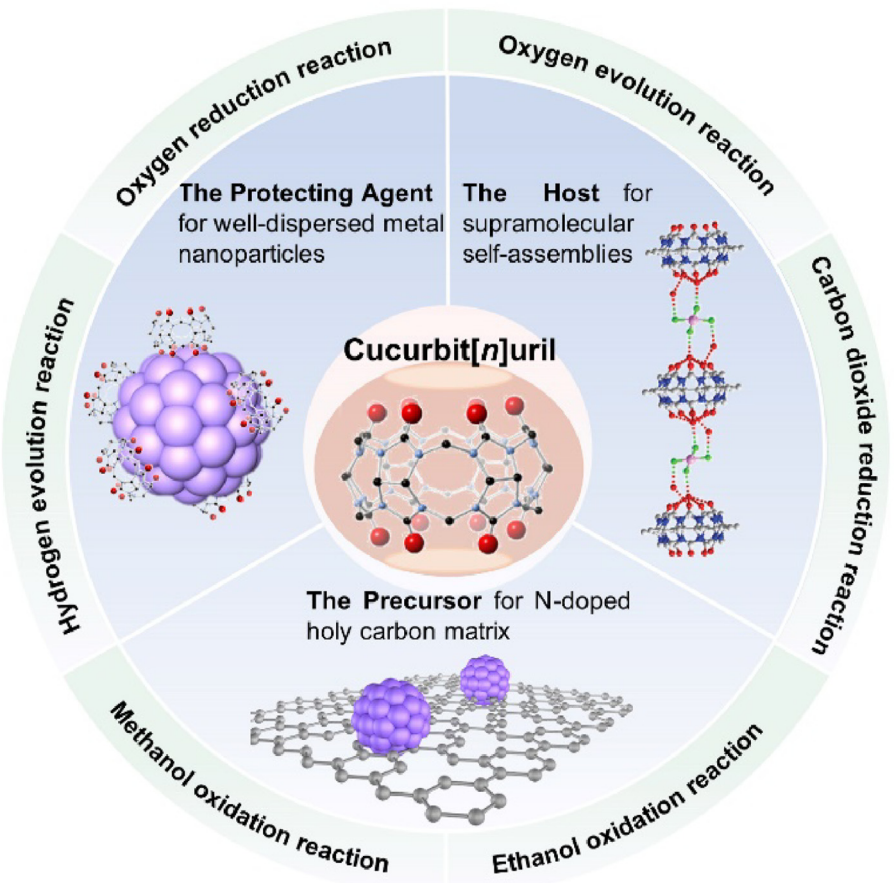

Fig. 3. A summary of the roles of CB[n]s in various electrocatalyses.

A lot of studies have revealed that the hydrated amorphous oxyhydroxides with $Ir^{3/4+}$ and uncoordinated O/Ir atoms (IrO_x) show superior activity for OER. However, it is still a big challenge that the Ir nanocatalysts construct with the surface of controllable Ir oxide composition and maintain such composition during catalytic processes. Using CB[6] as a protecting agent, CB[6]-Ir NPs with controllable surface Ir oxidation composition have been successfully prepared by reducing the Ir precursor in the presence of CB[6] with $NaBH_4$ in an ethanol/water mixture solution [29]. The fraction of surface-active IrO_x could be effectively adjusted by tuning the various proportions of CB[6] and Ir precursor. Thus, CB[6]-Ir (CB[6]-Ir1, CB[6]-Ir2, and CB[6]-Ir3) were obtained with different metal mass ratios of 2.0%, 3.0%, and 3.5%, respectively. Ir particles in the three samples were distributed uniformly with the similar size of 2.0 ± 0.2 nm, composed of face-centered cubic Ir for bulk verified by powder X-ray diffraction (PXRD), and the coexistence of Ir and IrO_x for surface tested by X-ray photoelectron spectroscopy (XPS) and X-ray absorption near-edge spectroscopy (XANES) (Fig. 4).

CB[6]-Ir2 performed the best among the three candidates, giving the highest activities for OER and HER as the overpotential were 270 mV and 54 mV, respectively, at a current density of 10 $mA \cdot cm^{-2}$ in 0.5 $mol \cdot L^{-1}$ H_2SO_4 electrolyte (Fig. 5). Moreover, CB[6]-Ir2 NPs could be seen as a bifunctional catalyst for extraordinary OER and HER catalytic performances in the acidic electrolyte. CB[6]-Ir2 NPs only required 1.56 V to achieve 10 $mA \cdot cm^{-2}$, which is among the highest activities reported. The CB[6]-Ir||CB[6]-Ir cell showed high stability of 20 h for continuous operation at 5 $mA \cdot cm^{-2}$ with less than a 5% potential increase. The authors attributed the remarkable performance to the coordination interaction between Ir atoms and CB[6]. This coordination interaction was identified by extended X-ray absorption fine structure (EXAFS) and electron energy loss spectroscopy (EELS). Moreover, DFT calculations verified that the electronic states of the Ir NPs surface were affected by the surface-adsorbed CB[6] molecules corresponding to XANES and XPS results. The computational results show that the lower O_2 affinity energy might be favorable with surface-active IrO_x and the Ir—O—C bonding as the dominating reasons for the enhanced activity and stability. Although few catalysts constructed with macrocycle were reported, this work will stimulate the metal-macrocycle molecule interactions that might be extendible to other electrocatalytic reactions.

Except for the role of CB[6] in the enhanced catalytic performance, CB[6] as a 3D molecule impacts the nucleation and growth kinetics of metal nanocrystals. In an early report, three sub-

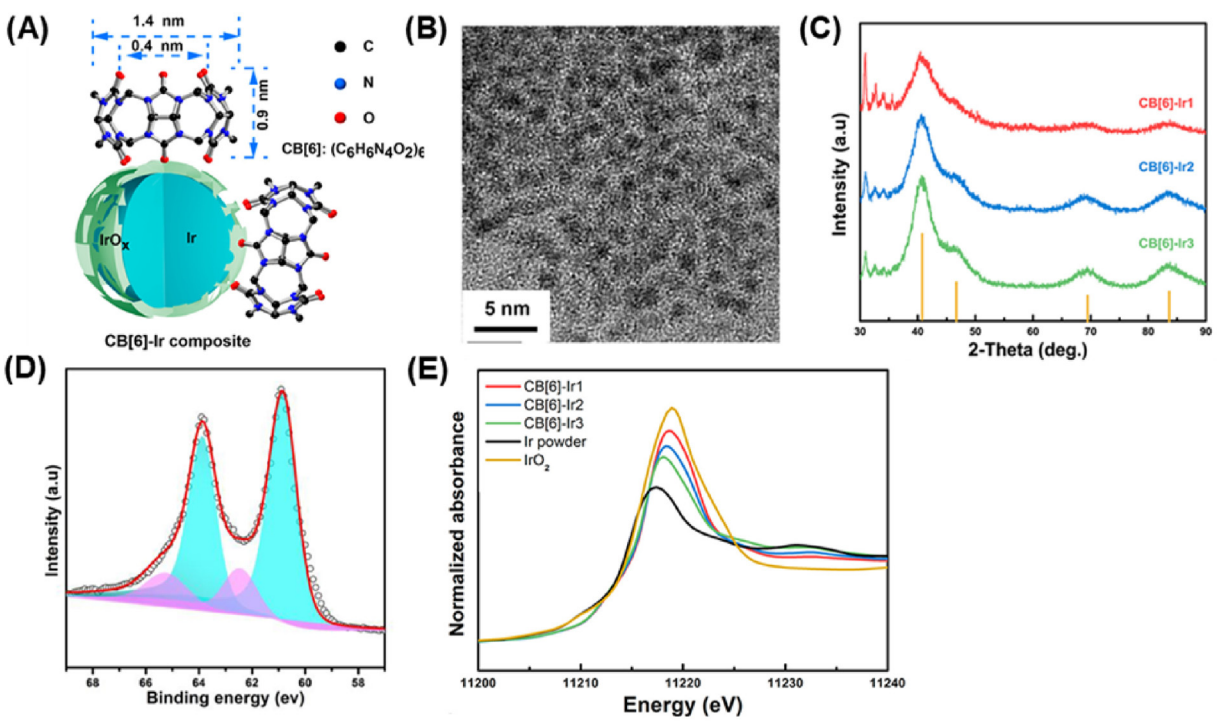

Fig. 4. (A) Conceptual picture of CB[6]-Ir composite. (B) HRTEM image and (D) Ir4f XPS of the as-prepared CB[6]-Ir2. (C) XRD patterns of the CB[6]-Ir catalysts. (E) XANES data on the Ir L_3-edge of the CB[6]-Ir composites, commercial Ir bulk powder, and IrO_2. Reproduced with permission of Ref [29]. Copyright 2019, American Chemical Society.

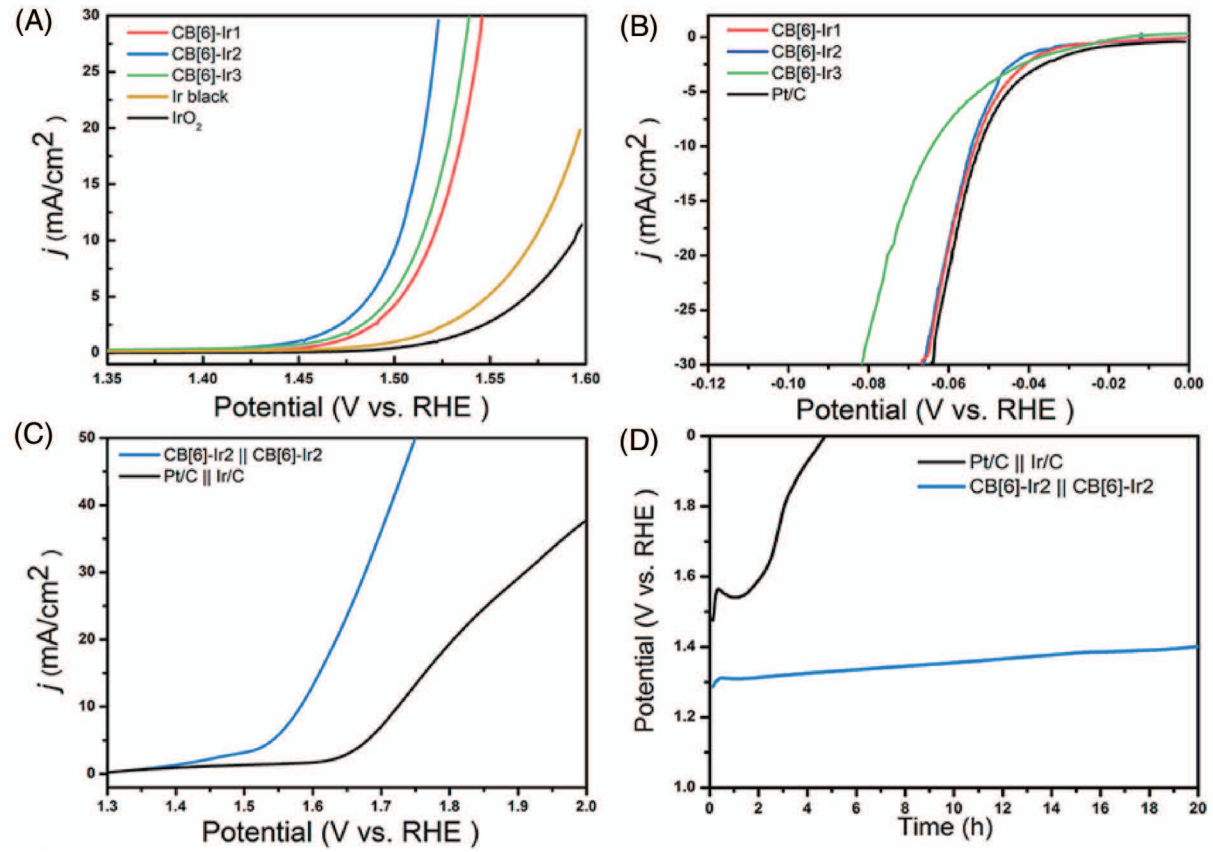

Fig. 5. (A) Polarization curves into the OER region of CB[6]-Ir composites, commercial Ir black, and IrO_2. (B) Polarization curves into the HER region of CB[6]-Ir composites and commercial Pt/C. (C) Polarization and (D) chronopotentiometric curves at 5 $mA{\cdot}cm^{-2}$ for overall water splitting of the CB[6]-Ir2||CB[6]-Ir2 and commercial Pt/C||Ir/C cells, respectively. Reproduced with permission of Ref [29]. Copyright 2019, American Chemical Society.

10 nm Pt NPs with distinctive shapes stabilized with CB[6] (CB[6]-Pt NP) were produced through the mediation of different components of reducing agents [30]. CB[6]-Pt NP with ethylene glycol (EG) and ascorbic acid (AA) exhibited enhanced activity for the methanol oxidation, and particularly the outstanding poisoning intermediates tolerance (Fig. 6). The activity improvement of Pt-based NPs is mainly owing to the multipod morphology exposed sufficient active sites in the large stepped surfaces obtained by the kinetic control with the co-reducing agents. The excellent poisoning tolerance of the CB[6]-Pt hybrids is attributed to the vital role of CB[6] that decreased the bonding strength between Pt and poisonous intermediates and thus facilitated the reaction. This strategy provides a simple and an effective route to develop Pt-based NPs through simple physical mixing with CB[6] for high electrocatalytic performance, and can also be potentially extended to other metals.

Our group reported that CB[6] capped Pd nanocubes (CB[6]-Pd NCs) in various sizes prepared by changing the ratio of CB[6] to metal precursors through wet-chemistry methods [31]. The colloidal synthesis of nanocrystals in controllable and uniform morphology extensively requires the assistance of capping agents for controlling the growth of crystal facets and thus the surface structure of the results. The most typical one is polyvinylpyrrolidone (PVP) polymer. However, PVP as a strong surfactant covers the active sites and then deteriorates the catalyst performance. Although some methods can remove PVP adsorbed on the catalyst surface, the morphologic destruction of nanocrystals, as well as the evitable aggregation of metal NPs might occur during the complicated post-treatment. For the first time, Pd NCs could be successfully synthesized with CB[6] instead of PVP due to the similar carbonyl functional group (Fig. 7). Compared with the surfactant-free commercial Pd black, commercial Pd/C, and PVP-Pd NCs, CB[6]-Pd NCs had the best electrocatalytic activity and stability toward ethanol oxidation reaction (EOR). Especially, the oxidation peak potential of CB[6]-Pd NCs was −233 mV, which is more negative than others, and the durability of the CB[6]-Pd NCs maintained 17 h of potential cycling. The reason why CB[6]-Pd NCs

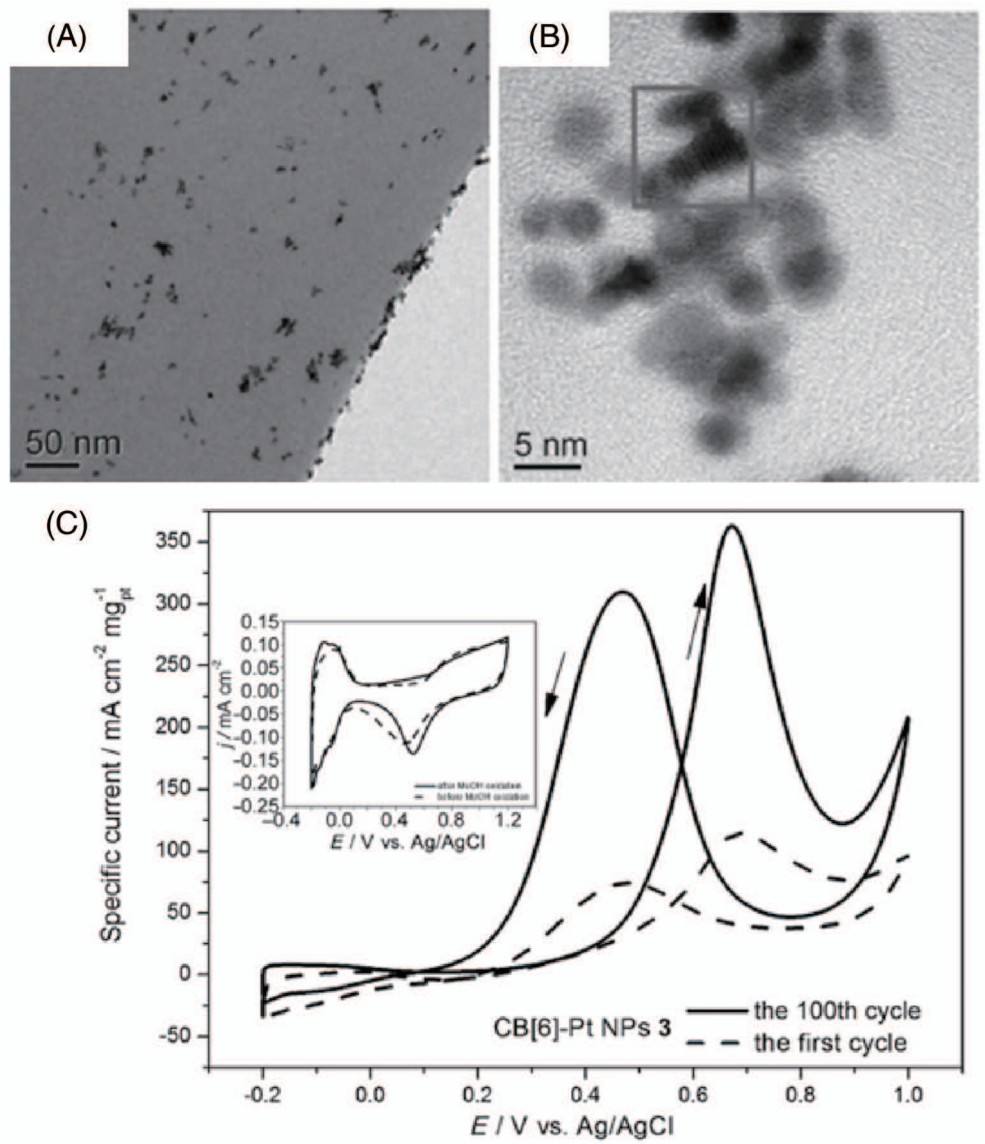

Fig. 6. (A) TEM and (B) HRTEM images of CB[6]-Pt NP. (C) The 1st and the 100th cyclic CVs of CB[6]-PtNP for methanol oxidation (the inset shows the corresponding CVs in 0.5 mol·L^{-1} H_2SO_4 before and after 100 potential cycles in methanol). Reproduced with permission of Ref [30]. Copyright 2012, John Wiley.

had the best electrocatalytic efficiency was that rigid macrocyclic structured CB[6] provided a steric effect that controlled the Pd cubes with a uniform size of sub-5 nm and leaves bare catalyst surfaces to ensure the high electrochemically active surface area for ORR. Besides, the electronic interaction between CB[6] and Pd NCs weakened the adsorption of poisoning CO species, which in turn released more active sites and promoted the reaction. Hence, more active sites due to CB[6] as the weak but effective protecting agent instead of PVP participated in ORR enhanced the catalytic activity and stability. This work points out a new protocol relied on macrocycle molecules to play a vital role in controlling the morphologies of metal nanocrystalline.

CB[6] as a weak protecting agent for controlling the morphology of metal nanocrystalline has also been demonstrated for the well-dispersed multipod Pd NPs [32]. The multipod Pd NPs stabilized by CB[6] (multipod Pd-CB[6]) were prepared by $PdCl_2$ reduction with oleylamine (OAm), 1-octadecylene (ODE), in the presence of CB[6] as a co-protecting agent. The multipod Pd-CB[6] showed great potential as an electrocatalyst toward both anodic EOR and cathodic ORR of fuel cells. DEFCs have been seen as environmentally friendly energy conversion devices with high efficiency and are convenient to transport and handle. The commercial Pd nanocatalysts are troubled by poor activities, weak stabilities, and low tolerance to reaction intermediates, so an urgent requirement is the

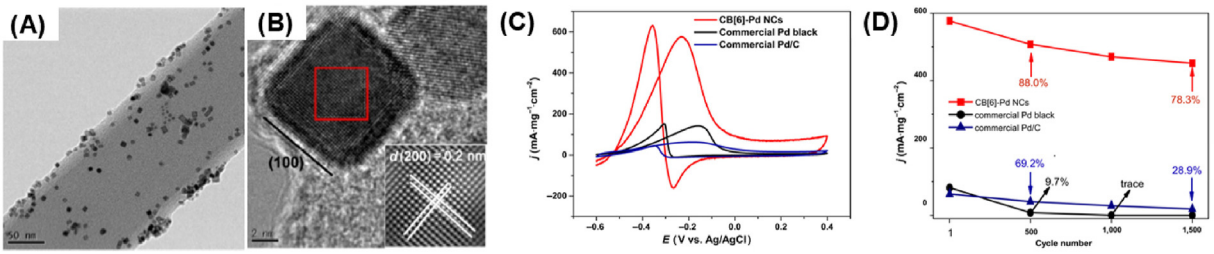

Fig. 7. (A) TEM and (B) HRTEM images of CB[6]-Pd NCs, the inset is the enlarged image of the selected red square area. (C) CVs and (D) forward peak current densities recorded every 500 cycles for the CB[6]-Pd NCs, commercial Pd black and commercial Pd/C in 0.1 mol·L^{-1} KOH + 0.1 mol·L^{-1} EtOH solutions. Reproduced with permission of Ref [31]. Copyright 2019, Springer Nature.

efficient Pd-based nanomaterials developed in DEFCs. The well-defined multipod structure stabilized by CB[6] in this work showed exceptionally enhanced performance for high ECSA and further enabled the studies on the interaction between CB [6] and metal nanocrystals in these reactions. Even if multipod Pd-CB[6] and multipod Pd were in similar shape and size observed from TEM images, and composed of metallic Pd confirmed by PXRD (Fig. 8), multipod Pd-CB[6] exhibited enhanced activity as the peak current for EOR was 10.3 mA·cm^{-2}, about 1.8 and 3.0 times than those of multipod Pd and commercial Pd/C, respectively, and the best durability with CB[6] protected (Fig. 9). Moreover, when evaluated as electrocatalysts toward ORR in O_2-saturated 0.1 mol·L^{-1} KOH electrolyte, multipod Pd-CB[6] exhibited the best mass activity, and especially the longest stability for 36,000 s. The improvement can be ascribed to the interaction between the catalytic particles and CB[6] corresponding to the increasing percentage of Pd^{2+} of the nanocrystal surface and a redshift of the carbonyl peak verified by XPS and infrared (IR) spectroscopic analysis. This work provides a broader perspective for developing well-stabilized Pd NPs with CB[6] with good electrochemical activity and stability in fuel cells.

Apart from the interaction between metal nanoparticles and CB[6] facilitating the activity and stability for various catalytic reactions in the above works, a third component introduced provides the potential to break through the bottleneck. The catalysts for environmentally friendly HER over the whole pH range have attracted much attention but usually suffer from low durability and high

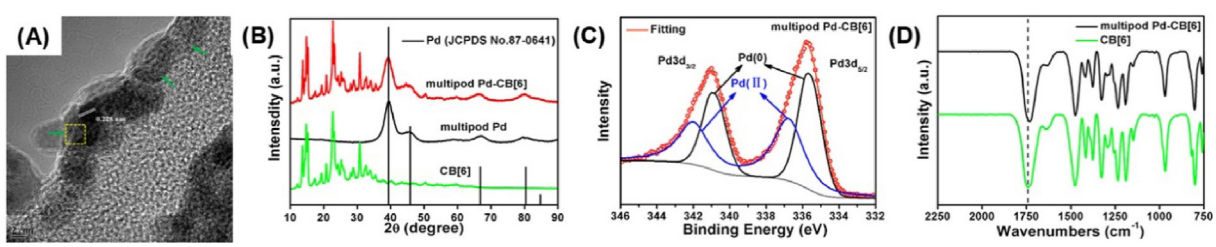

Fig. 8. (A) HRTEM image and (C) Pd 3d XPS spectrum of multipod Pd-CB[6]. (B) PXRD patterns of multipod Pd-CB[6], multipod Pd, and CB[6]. (D) IR spectra of multipod Pd-CB[6] and CB[6]. Reproduced with permission of Ref [32]. Copyright 2020, American Chemical Society.

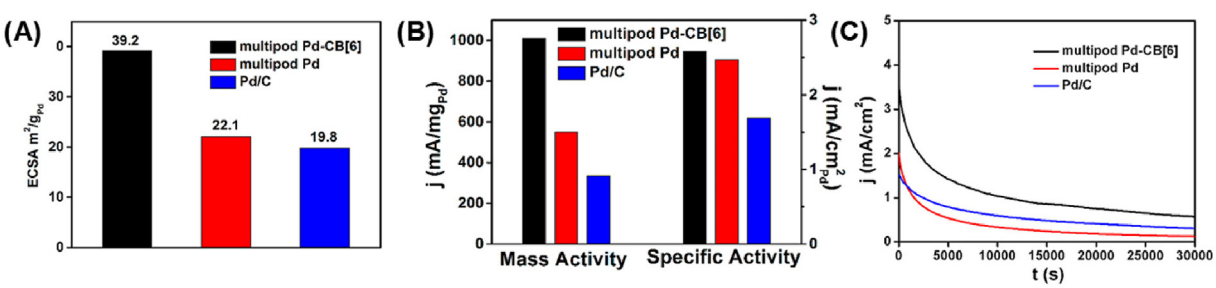

Fig. 9. (A) Histograms for ECSAs of multipod Pd-CB[6], multipod Pd, and commercial Pd/C performed in 0.1 mol·L^{-1} KOH solution. (B) Mass activities and specific activities of samples for EOR. (C) Chronoamperometric curves of EOR. Reproduced with permission of Ref [32]. Copyright 2020, American Chemical Society.

overpotential. Our group reported well-dispersed Ru nanoclusters (Ru NCs) on thin reduced graphene oxide stabilized by CB[6] (Ru-CB[6]/rGO) through a simple solvothermal method [33]. With the protection of CB[6], the ultrafine Ru NCs with the size of ca. 1.9 nm uniformly distributed on the rGO nanosheets (NSs) with the thickness of 3.4 nm, avoiding stacking observed by TEM and atomic force microscopy (AFM) (Fig. 10). The ternary nanohybrid showed superior performance in that the overpotentials at -10 mA·cm^{-2} were only 44, 72, and 48 mV in acidic, alkaline, and neutral media, respectively, which are much higher than those of other binary candidates. For the stability in an acidic solution, the advantage for Ru-CB[6]/rGO became obvious for 24 h with just 19 mV decline, while the overpotential of commercial Pt/C lost 221 mV after only 8 h test (Fig. 11). The improvement can be attributed to the intrinsic characteristic of the Ru NCs with abundant active sites and rGO nanosheets with the charge transfer promotion and the protection of CB[6] for the maximum of those advantages to effectively prevent the catalyst from poisoning. This strategy by the addition of the third part endows the enhancement for the wider application, and the protection of CB[6] ensures the high stability of the catalysts.

3. Cucurbit[*n*]uril-based supramolecular self-assemblies for electrocatalysis

Except for the synthesis of the metal nanomaterials through the physical mixing of metal precursors with CB[6], another sophisticated strategy via the supramolecular self-assembly of CB[*n*] and metal was also developed for the exploitation of the electrocatalysts.

It was reported that well-dispersed ultra-small Pd NPs (Pd-Me_{10}CB[5]) with the size of ca. 2.4 nm were successfully obtained through the thermal reduction of $[(H_2O)_2(Me_{10}CB[5]@H_2O)]\cdot[PdCl_4]\cdot 3H_2O\cdot(PdCl_4\text{-}Me_{10}CB[5])$ (Fig. 12) [34]. The unique supramolecular self-assembly was composed of macrocyclic decamethylcucurbit[5]uril (Me_{10}CB[5]) and $[PdCl_4]^{2-}$ though H-bonding obtained by the diffusion method in the H-shape tube and then used as the catalyst for the electrocatalytic CO_2

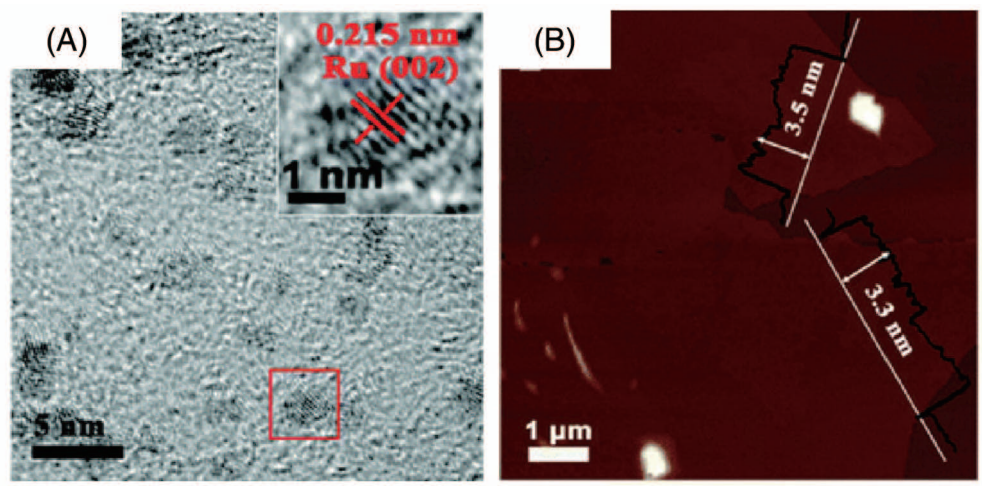

Fig. 10. (A) HRTEM and (B) AFM images of Ru-CB[6]/rGO. Reproduced with permission of Ref [33]. Copyright 2020, Royal Society of Chemistry.

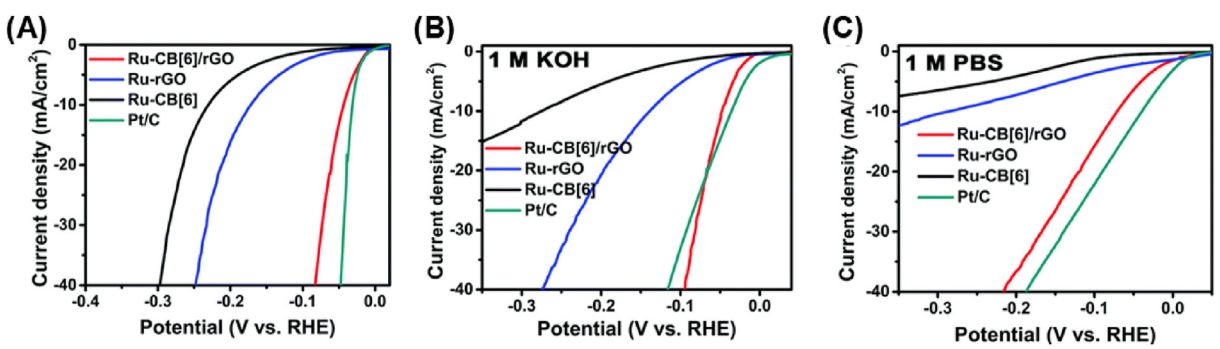

Fig. 11. Polarization curves of different catalysts in (A) 0.5 mol·L^{-1} H_2SO_4, (B) 1 mol·L^{-1} KOH and (C) 1 mol·L^{-1} PBS. Reproduced with permission of Ref [33]. Copyright 2020, Royal Society of Chemistry.

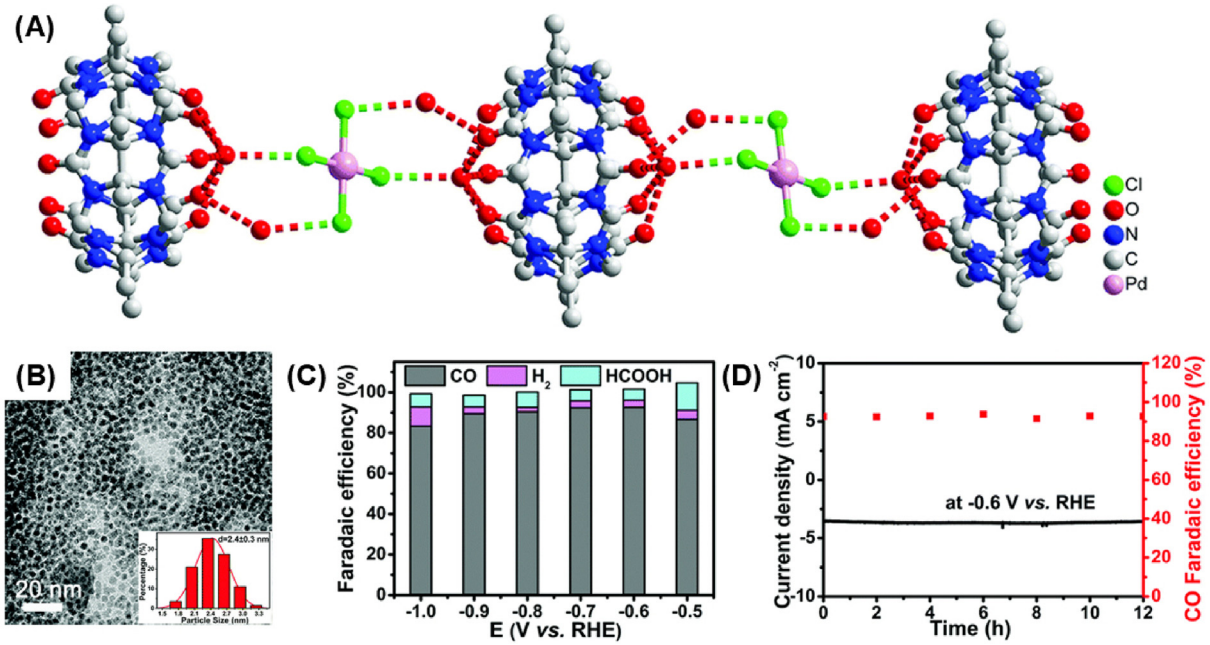

Fig. 12. (A) The one-dimensional chain subunit of $PdCl_4$-Me_{10}CB[5]. (B) TEM image of Pd-Me_{10}CB[5]. (C) FEs of CO, H_2 and HCOOH measured and (D) stability performance operated at −0.6 V for 12 h over Pd-Me_{10}CB[5] in CO_2-saturated 0.5 mol·L^{-1} $KHCO_3$ solution. Reproduced with permission of Ref [34]. Copyright 2019, Royal Society of Chemistry.

reduction reaction (CO_2RR). The electro-reduction of CO_2 as a promising method to produce chemicals and fuels has attracted increasing interest but is limited by the large energy barrier and the superiority of competitive HER. Pd-based nanocatalysts are efficient in CO_2RR to CO due to the strong binding energies for the intermediates. The obtained ultra-small Pd NPs were evenly loaded on Me_{10}CB[5], showing excellent catalytic selectivity for CO as the maximum FE_{CO} reached 92.5% at −0.6 V *vs.* RHE in 0.5 mol·L^{-1} $KHCO_3$ and the stability lasted for 12 h. Such catalytic properties far outperformed the commercial Pd/C catalyst, which was attributed to the role of rigid macrocyclic Me_{10}CB[5] as a stabilizer and support to bare more low-coordinated surface atoms favored with reaction intermediates verified by the high ECSA value. The distinctive method in this work of the preparation of Pd-based nanocatalyst for CO_2RR to CO may be extended to the other nano-sized metal catalysts.

Our group also reported Au NPs (CB[*n*]-Au NPs) with a size of ca. 4 nm through a similar method for the reduction of the supramolecular assemblies composed of $[AuCl_4]^-$ and macrocyclic Me_{10}CB[5], and cucurbit[*n*]urils (CB[*n*]s, n = 5, 6, 8) (Fig. 13) [35]. Me_{10}CB[5]-Au NPs exhibited the highest selectivity for CO as the FE_{CO} achieved 93.2% at −0.6 V *vs.* RHE in 0.5 mol·L^{-1} $KHCO_3$ and CB[6]-Au NPs showed comparable selectivity as the FE_{CO} reached 91.6% and superior stability for 72 h. The enhanced performance was ascribed to the high-density uncoordinated surface atoms of Au NPs as the abundant active sites. Moreover, the CB[*n*] macrocycles ensure the formation of ultra-small Au NPs. During the reaction, the CB[*n*] macrocycles could effectively protect nanoparticles from aggregation, then directly modulate the affinity to the intermediates to facilitate the CO_2RR and inhibit the rival HER. This work proves an effective strategy for the exploitation of CB[*n*]-based catalysts for various electrochemical reactions.

Additionally, the third composition except CB[*n*] and metal NPs of supramolecular assembly could play an important role in the catalytic performance. Our group reported a series of Pt-based supramolecular assemblies (M$PtMe_{10}$CB[5], M = Na, K, Rb, or Cs) with an alkali metal ion to coordinate with Me_{10}CB[5] through the slow diffusion method and tested as an electrocatalyst for ORR in acidic media (Fig. 14) [36]. Single-crystal X-ray diffraction characterization indicated the different space groups with the various alkali metals, which caused the diverse electron structure of the adjacent Pt atom revealed by the DFT investigations. When performed in an electrolyte of 0.1 mol·L^{-1} $HClO_4$, the catalytic activities of various M$PtMe_{10}$CB[5] toward ORR were found to follow the order of Cs < Rb < K < Na. The NaPt-Me_{10}CB[5] catalyst showed the best performance with a half-wave potential of 0.713 V, and a limiting diffusion current density of 6.63 mA·cm^{-2} which

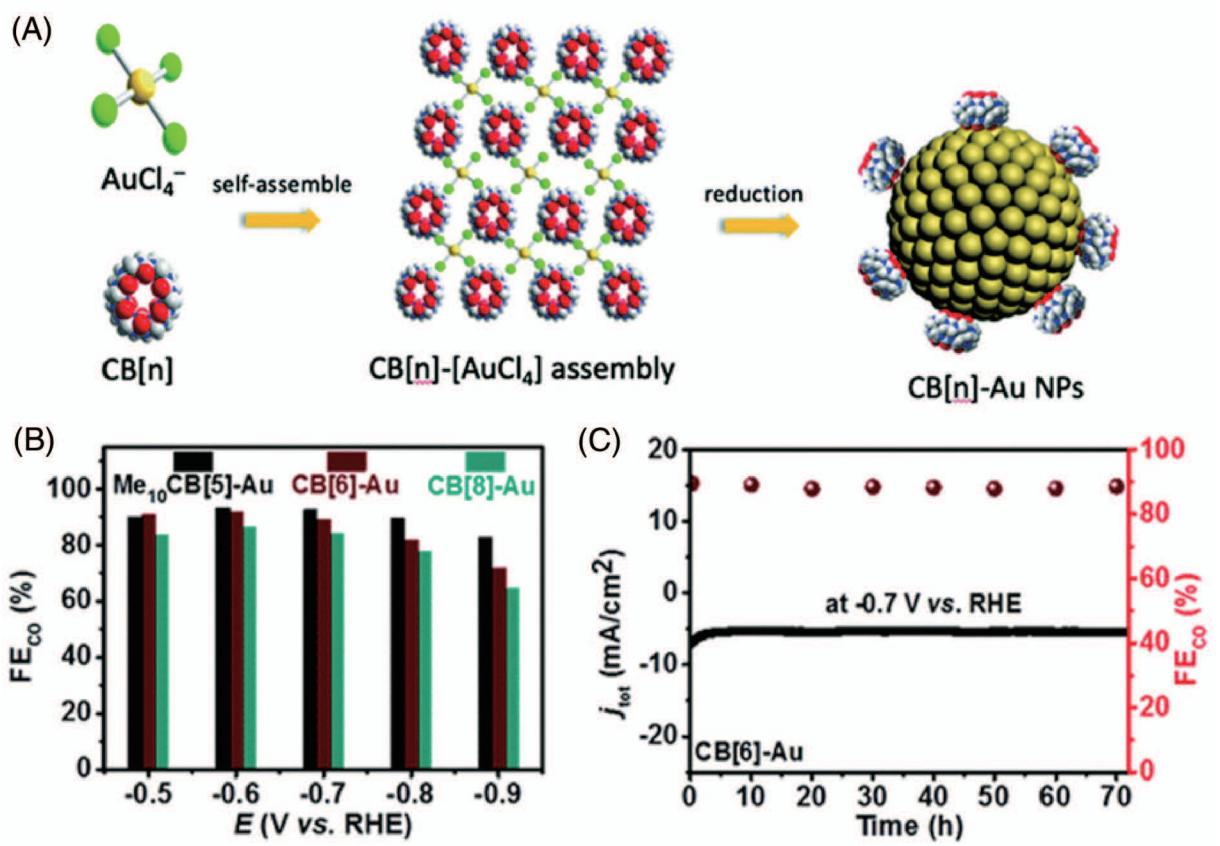

Fig. 13. (A) Schematic illustration for the preparation processes of the CB[n]-Au NPs to form supramolecular assemblies (CB[n] = Me_{10}CB[5], CB [6] and CB[8]). (B) CO faradaic efficiencies for the supramolecular assemblies. (C) Stability performance of the CB[6]-Au NPs operated at 0.7 V in CO_2-saturated 0.5 mol·L^{-1} $KHCO_3$. Reproduced with permission of Ref [35]. Copyright 2021, Royal Society of Chemistry.

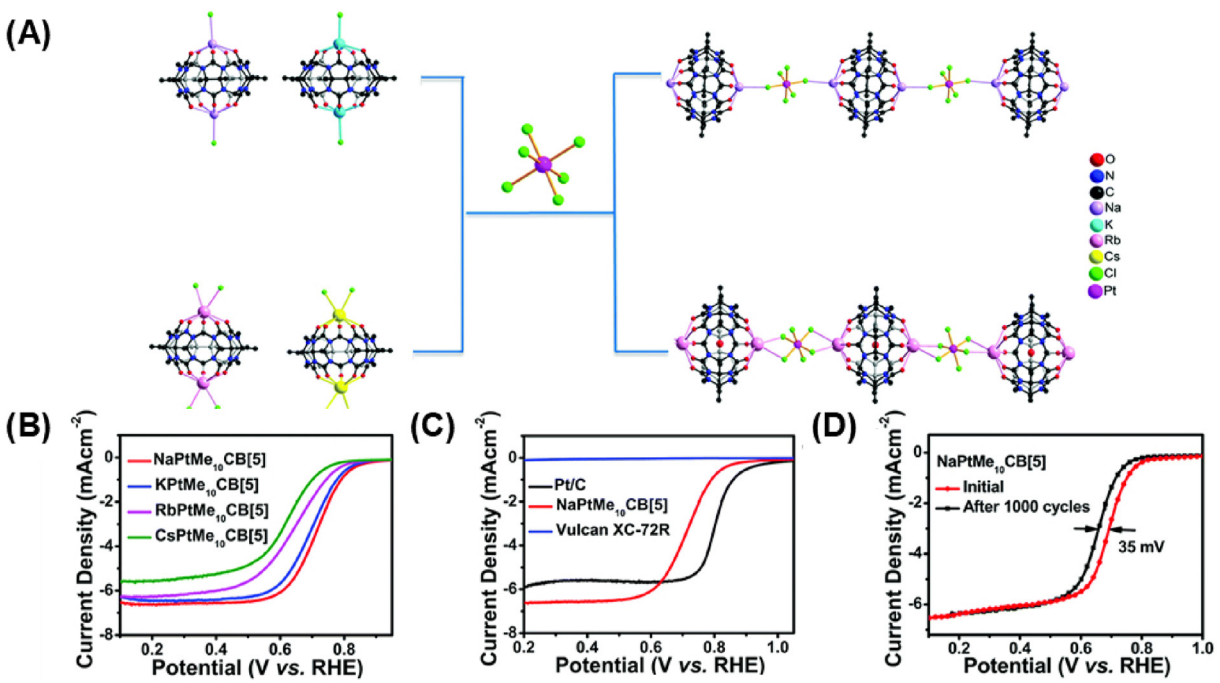

Fig. 14. (A) The molecular capsule of M-Me_{10}CB[5] (M = Na, K, Rb and Cs), constructed by Me_{10}CB[5] coordinated to various alkali metal ions, and the one-dimensional structure of $MPtMe_{10}$CB[5]. (B) Polarization curves recorded for $MPtMe_{10}$CB[5] (M = Na, K, Rb and Cs). (C) Polarization curves recorded for $NaPtMe_{10}$CB[5], Vulcan XC-72R and the commercial 20 wt% Pt/C catalyst. (D) The accelerated durability tests of $NaPtMe_{10}$CB[5]. Reproduced with permission of Ref [36]. Copyright 2019, Royal Society of Chemistry.

was closed to those of the commercial Pt/C catalyst, and kept stable over 1000 cycles. This enhancement was attributed to the optional charge population of the active sites modulated by the alkali metal and the good resistance of the supramolecular assemblies with CB[*n*]. This work opens a new protocol for the third composition such as alkali metals introduced in the metal-CB[*n*] compound to broaden the electrocatalytic applications.

This promising approach of CB[*n*] assembled with the third part provides the potential to exceed the catalytic performance of other homologs. A new covalent organic framework (COF-TPP-CB[6]) was obtained based on perpropargyloxy CB[6] assembled with TPP-Zn-4N_3 [37]. To enhance the HER performance, a small amount of Ni was introduced as the cocatalyst. 12%Ni@COF-TPP-CB [6] with 12% Ni loading showed great HER catalytic property as 18.7 $mmol \cdot g^{-1} \cdot h^{-1}$ of hydrogen. In another work, CB[8] was used to construct a two-dimensional polypseudorotaxane as the platform for the preparation of Pt NPs (PtNPs@(CB[8]/DMV/TPP-Np)) [38]. The sample was efficiently applied in the electrochemical synthesis of nitrogen reduction to ammonia with a high yield.

Moreover, supramolecular self-assemblies could provide a promising strategy in the lithium battery application. CB[6] was reported as a supramolecular capsule in lithium-sulfur (Li-S) batteries [39]. The battery equipped with CB[6] showed a greatly improved capacity from 300 to 900 $mAh \cdot g^{-1}$. This improvement was attributed to the abundant adsorptive sites on CB[6] to ensure the store and release of lithium polysulfides (LiPSs). Subsequently, an unconventional supramolecular electrolyte (SSE) was obtained based on CB[6] assembled with Li salts [40]. SSE exhibited a great Li ion conductivity of 2.9×10^{-4} $S \cdot cm^{-1}$ at room temperature (25 °C), which benefited from moderate bonding energies and suitable Li chemical environments. Hence, it is confirmed that supramolecular self-assemblies have the potential to construct well-performed materials for electrochemical application.

4. Cucurbit[*n*]uril as precursor for the preparation of carbon matrix

The pyrolysis method for providing N-doped carbon material is a conventional approach to fabricating electrocatalysts. The most frequently-used precursor is the mixture of carbon sources (such as carbon tubes [41], graphene [42], and graphite [43]) and nitrogen sources (such as urea [44]). However, the separated C and N sources lead to the uneven distribution of N in the carbon lattice. To solve this problem, metal-organic frameworks and mesoporous silica are recently utilized to produce N-doped carbon material, but some resident elements from these templates require a post-treatment. Therefore, it is important to develop a new precursor for the N-doped carbon matrix.

Our group reported that the macrocycle CB[6] was utilized as the precursor to prepare N-doped holey carbon (NHC) (Fig. 15) [45]. CB[6] is featured with a metal-free and rigid porous backbone, together with high N content (34%). After the high temperature pyrolysis procedure, the N-doped carbon showed inherent abundant N content and in-plane holes. The nitrogen-sorption isotherms at 77 K showed that NHCs exhibited Type-IV isotherms with a hysteresis loop, indicating the existence of micro- and mesopores. The obtained NHCs from CB[6] were then utilized for ORR process. NHC-800 (pyrolysis temperature of 800 °C) exhibited the best activity (onset potential of 0.88 V), higher than the commercial Pt/C. Moreover, NHC-800 showed good stability and methanol tolerance. The satisfactory performance of NHC could be attributed to its porous structure, abundant active N-species, and in-plane holes. This is the first report on preparing NHC with cucurbit[*n*]urils, which presents an encouraging catalog of precursors to afford a functional carbon matrix.

Furthermore, CB[6] was developed as the precursor to prepare atomically dispersed metal-doped carbon electrocatalysts. The Fe-doped

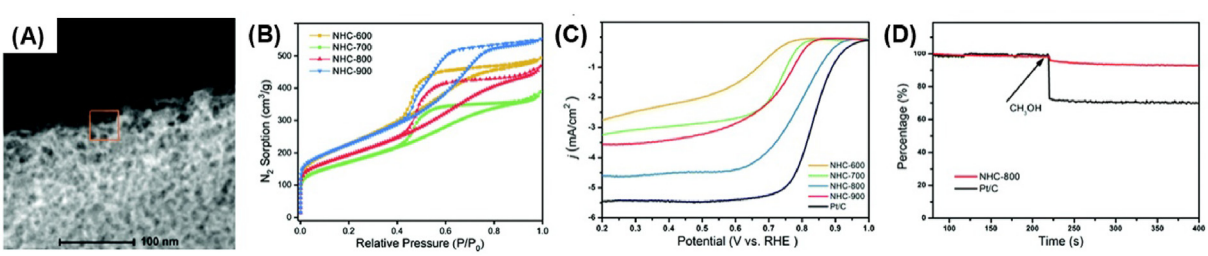

Fig. 15. (A) A HADDF-STEM image of NHC-800. (B) Nitrogen sorption isotherms of NHCs. (C) LSV curves of NHCs and 20 wt% Pt/C catalyst. (D) Methanol tolerance testing curves of NHC-800 and Pt/C at the RHE working potential. Reproduced with permission of Ref [45]. Copyright 2019, Royal Society of Chemistry.

carbon (SC-Fe) electrocatalyst was firstly synthesized [46]. Fe atoms were well dispersed on the porous carbon from the pyrolyzation of CB[6] without the template synthesis. Compared with the supramolecule-derived carbon (SC) catalyst, the SC-Fe catalyst exhibited greatly enhanced property for ORR. For SC-Fe, the half-wave potential was 0.869 V, which was 100 mV higher than SC. The improvement suggested the well dispersed Fe atoms as the active sites for ORR.

Afterward, a series of M-N-C single-atom electrocatalysts were obtained and exhibited excellent ORR performance in another work [47]. After pyrolyses of CB[6] and Fe (Co, Ni) chloride at 900 °C, Fe-NHC, Co-NHC, and Ni-NHC single-atom electrocatalysts could be fabricated (Fig. 16). The HAADF-STEM image showed the holey structures over the whole carbon matrix, which promotes the homogeneous dispersion of metal sites. Moreover, the isolated Fe metal sites were confirmed by aberration-corrected high angle annular dark-field scanning transmission electron microscopy (AC-HAADF-STEM). N_2 adsorption-desorption analysis proved the existence of a hierarchical micro/mesoporous structure, which is indispensable for the generation of an ample electrode/electrolyte interface for ion or charge accumulation performance during the ORR. The three catalysts were tested for ORR, which showed that Fe-NHC has the best performance, better than Co-NHC, Ni-NHC, and commercial Pt/C. Inspired by this result, Fe-NHC was further employed for the Zn-air battery, and was able to achieve higher power and energy density with longer-term stability than Pt/C + Ir/C catalyst. This work demonstrates the potential and advantages of fabricating single-atom catalysts by pyrolysis of porous substrates, such as CB[6].

As a promising replacement for Pt-based ORR catalysts, transition metal carbides (TMCs) have similar electronic structures to Pt near the Fermi level, excellent electrical conductivity, high oxidation resistance, and good methanol or CO tolerant capability [48]. It is of great significance to develop suitable support for nanosized TMC. Using CB[6] and melamine (MA) together as carbon precursors, the obtained NHC featured abundant defective sites and high nitrogen content, which is ideal support for TMC. Phosphomolybdic acid, CB[6], and MA were first mixed and treated to produce mel/CB[6]/PMo_{12}, then pyrolysis of this precursor produced the Mo_2C/NHC composite. TEM images illustrated that Mo_2C NPs with an average size distribution of 1.5 nm were uniformly distributed on the NHC matrix (Fig. 17). Raman spectra indicated that the introduction of MA generates more defects. In the ORR reaction, Mo_2C/NHC is comparable to that of noble metal Pt/C benchmark catalyst with an initial potential (0.95 V), half-wave potential (0.84 V), and limiting current density (5.0 mA·cm^{-2}). Thanks to the strong interaction between the Mo_2C NPs and the carbon support, the Mo_2C/NHC exhibited good long-term durability, maintaining 77.21% current density after 25 h chronoamperometric (CA) testing. This work firstly showed the advantage of cucurbit[n]urils to fabricate TMCs as a cost-effective electrocatalyst with high catalytic activity and outstanding long-term durability.

Except for ORR, metal-doped carbon electrocatalysts show great potential for HER. A series of Iridium-doped mesoporous carbon (CBC-Ir)

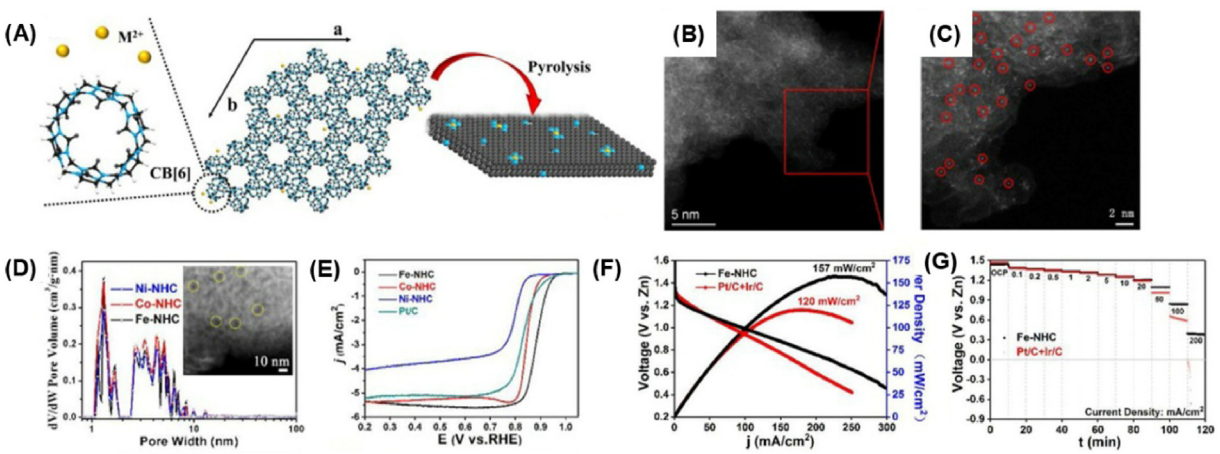

Fig. 16. (A) Schematic illustration of the preparation of CB[6]-derived M-N-C single-atom catalysts (In the structure of a single CB[6] molecule, gray, black, blue and white represent O, C, N, and H, respectively.) (B) AC-HAADF-STEM image and (C) enlarged image of Fe-NHC (Some Fe single atoms are highlighted by red circles). (D) Pore size distribution curves of CB[6]-derived M-N-C catalysts. (E) LSV curves of CB[6]-derived M-N-C and Pt/C catalysts. (F) Discharge polarization curves and corresponding power density curves employing Fe-NHC or Pt/C + Ir/C catalysts for air electrode. (G) Testing for open-circuit voltage and rate discharge curves of assembled ZABs using Fe-NHC and Pt/C + Ir/C catalysts at different current densities. Reproduced with permission of Ref [47]. Copyright 2021, Elsevier.

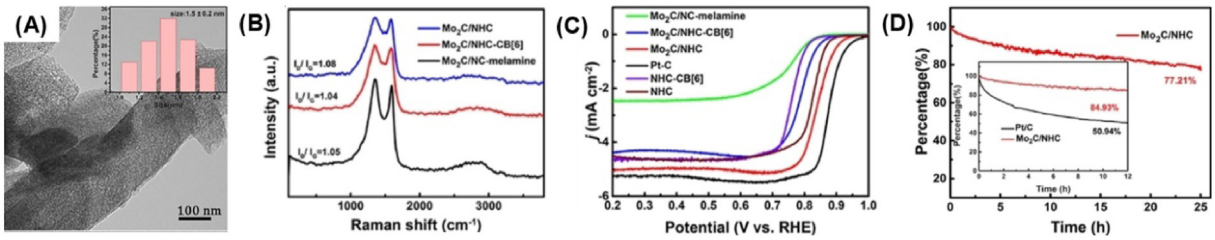

Fig. 17. (A) TEM images of the Mo_2C/NHC sample. (B) Raman patterns of Mo_2C/NHC, Mo_2C/NHC-CB[6], and Mo_2C/NC-melamine. (C) LSV curves and (D) Chronoamperometric responses of Mo_2C/NHC and Pt/C at a constant potential of 0.7 V in O_2-saturated 0.1 mol·L^{-1} KOH electrolytes. Reproduced with permission of Ref [48]. Copyright 2022, John Wiley.

materials were prepared based on CB[6] as the carbon precursor with various pyrolysis temperatures [49]. Among them, the CBC-Ir-800-1.2 catalyst exhibited superior performance as the overpotentials of 17 and 33 mV in acid (0.5 mol·L^{-1} H_2SO_4) and alkaline (1.0 mol·L^{-1} KOH) electrolytes at 10 mA·cm^{-2}, respectively. This HER performance even surpassed that of commercial Pt/C catalyst (28 and 43 mV). It is an encouraging approach of introducing supramolecular macrocycles as the abundant N-doped carbon backbone for synthesizing excellent electrocatalysts.

5. Conclusions and perspectives

In this review article, we have discussed how the cucurbit[*n*]urils (CB[*n*]) played the role in metal nano electro-catalysts. The CB[*n*]-metal composites, which integrate the merits of both greatly stable CB[*n*]s and highly reactive nanocatalyst, have been successfully synthesized by various protocols, such as wet-chemistry and diffusion methods. Moreover, the N-doped holey carbon matrixes obtained by the pyrolysis of CB[*n*]s have been verified as a promising support for the single atoms or the clusters. For the role of CB[*n*]s in the enhancement of activity, it could expose sufficient active sites and maintain the favorable metal oxidation state in the surfaces. Furthermore, the enhancement of stability can be attributed to the maintenance of morphology and dispersion of the nanomaterials owing to CB[*n*]s.

However, there are very limited reports on such CB[*n*]-metal composites and some challenges have to be faced. For example, the bonding interactions between CB[*n*]s and metal nanomaterials are so complicated that few characterization methods could demonstrate it accurately from the molecular level. The relationship between the performance and the inner structure of the catalytic system is not clear enough. Thus, the development is proceeding slowly, but has great opportunities.

In the end, it is important to have a good understanding of such interaction, which is greatly helpful for the construction of new CB[*n*]-based metal nanomaterials. We expect that a novel strategy of nanocatalysts stabilized by CB[*n*]s could overcome the challenges, and develop more efficient catalysts to be applied for broader electro-applications.

Acknowledgements

We appreciate the financial supports from the National Key Research and Development Program of China (2018YFA0704502), the National Natural Science Foundation of China (NSFC) (22033008) and Fujian Science & Technology Innovation Laboratory for Optoelectronic Information of China (2021ZZ103).

References

[1] Nitopi S, Bertheussen E, Scott S B, Liu X Y, Engstfeld A K, Horch S, Seger B, Stephens I EL, Chan K, Hahn C, Norskov J K, Jaramillo T F, Chorkendorff I. Progress and perspectives of electrochemical CO_2 reduction on copper in aqueous electrolyte[J]. Chem. Rev., 2019, 119(12): 7610−7672.

[2] Jiang X, Nie X W, Guo X W, Song C S, Chen J G G. Recent advances in carbon dioxide hydrogenation to methanol via heterogeneous catalysis[J]. Chem. Rev., 2020, 120(15): 7984−8034.

[3] Zheng Y, Jiao Y, Vasileff A, Qiao S Z. The hydrogen evolution reaction in alkaline solution: from theory, single crystal models, to practical electrocatalysts[J]. Angew. Chem. Int. Ed., 2018, 57(26): 7568−7579.

[4] Wu Z P, Lu X F, Zang S Q, Lou X W. Non-noble-metal-based electrocatalysts toward the oxygen evolution reaction [J]. Adv. Funct. Mater., 2020, 30(15): 1910274.

[5] Feng Y C, Wang X, Wang Y Q, Yan H J, Wang D. *In situ* characterization of electrode structure and catalytic processes in the electrocatalytic oxygen reduction reaction[J]. J. Electrochem., 2022, 28(3): 112−124.

[6] Tomboc G M, Choi S, Kwon T, Hwang Y J, Lee K Y. Potential Link between Cu surface and selective CO_2 electroreduction: perspective on future electrocatalyst designs [J]. Adv. Mater., 2020, 32(17): 1908398.

[7] Yao Q, Huang B L, Zhang N, Sun M Z, Shao Q, Huang X Q. Channel-rich RuCu nanosheets for pH-universal overall water splitting electrocatalysis[J]. Angew. Chem. Int. Ed., 2019, 58(39): 13983−13988.

[8] Mamtani K, Jain D, Dogu D, Gustin V, Gunduz S, Co A C, Ozkan U S. Insights into oxygen reduction reaction (ORR) and oxygen evolution reaction (OER) active sites for

nitrogen-doped carbon nanostructures (CN_x) in acidic media[J]. Appl. Catal., B, 2018, 220: 88−97.

[9] Liu M L, Zhao Z P, Duan X F, Huang Y. Nanoscale structure design for high-performance Pt-based ORR catalysts[J]. Adv. Mater., 2019, 31(6): 1802234.

[10] Zhuang Z H, Chen W. Application of atomically precise metal nanoclusters in electrocatalysis[J]. J. Electrochem., 2021, 27(2): 125−143.

[11] Loiudice A, Lobaccaro P, Kamali E A, Thao T, Huang B H, Ager J W, Buonsanti R. Tailoring copper nanocrystals towards C_2 products in electrochemical CO_2 reduction[J]. Angew. Chem. Int. Ed., 2016, 55(19): 5789−5792.

[12] Huang J F, Hormann N, Oveisi E, Loiudice A, Gregorio G L, Andreussi O, Marzari N, Buonsanti R. Potential-induced nanoclustering of metallic catalysts during electrochemical CO_2 reduction[J]. Nat. Commun., 2018, 9: 3117.

[13] Qiu J C, Nguyen Q N, Lyu Z H, Wang Q X, Xia Y N. Bimetallic Janus nanocrystals: syntheses and applications [J]. Adv. Mater., 2022, 34(1): 2102591.

[14] Mahmood J, Li F, Jung S M, Okyay M S, Ahmad I, Kim S J, Park N, Jeong H Y, Baek J B. An efficient and pH-universal ruthenium-based catalyst for the hydrogen evolution reaction[J]. Nat. Nanotechnol., 2017, 12(5): 441−446.

[15] Wang H M, Chen Z N, Wu D S, Cao M N, Sun F F, Zhang H, You H H, Zhuang W, Cao R. Significantly enhanced overall water splitting performance by partial oxidation of Ir through Au modification in core-shell alloy structure[J]. J. Am. Chem. Soc., 2021, 143(12): 4639−4645.

[16] Lagona J, Mukhopadhyay P, Chakrabarti S, Isaacs L. The cucurbit[*n*]uril family[J]. Angew. Chem. Int. Ed., 2005, 44(31): 4844−4870.

[17] Brehrend R, Meyer E, Rusche F I. Ueber condensationsproducte aus glycoluril und formaldehyd[J]. Eur. J. Org. Chem., 1905, 339(1): 1−37.

[18] Freeman W A, Mock W L, Shih N Y. Cucurbituril[J]. J. Am. Chem. Soc., 1981, 103(24): 7367−7368.

[19] Kim S Y, Jung I S, Lee E, Kim J, Sakamoto S, Yamaguchi K, Kim K. Macrocycles within macrocycles: cyclen, cyclam, and their transition metal complexes encapsulated in cucurbit[8]uril[J]. Angew. Chem. Int. Ed., 2001, 40(11): 2119−2121.

[20] Zhao J Z, Kim H J, Oh J, Kim S Y, Lee J W, Sakamoto S, Yamaguchi K, Kim K. Cucurbit[*n*]uril derivatives soluble in water and organic solvents[J]. Angew. Chem. Int. Ed., 2001, 40(22): 4233−4235.

[21] Lee J W, Samal S, Selvapalam N, Kim H J, Kim K. Cucurbituril homologues and derivatives: new opportunities in supramolecular chemistry[J]. Acc. Chem. Res., 2003, 36(8): 621−630.

[22] Lee T C, Scherman O A. Formation of dynamic aggregates in water by cucurbit[5]uril capped with gold nanoparticles [J]. Chem. Commun., 2010, 46(14): 2438−2440.

[23] de la Rica R, Velders A H. Biomimetic crystallization of Ag_2S nanoclusters in nanopore assemblies[J]. J. Am. Chem. Soc., 2011, 133(9): 2875−2877.

[24] Cao M N, Lin J X, Yang H X, Cao R. Facile synthesis of palladium nanoparticles with high chemical activity using cucurbit[6]uril as protecting agent[J]. Chem. Commun., 2010, 46(28): 5088−5090.

[25] Cao M N, Wu D S, Su W P, Cao R. Palladium nanocrystals stabilized by cucurbit[6]uril as efficient heterogeneous catalyst for direct c−h functionalization of polyfluoroarenes [J]. J. Catal., 2015, 321: 62−69.

[26] Li H F, Lu J, Lin J X, Huang Y B, Cao M N, Cao R. Crystalline hybrid solid materials of palladium and decamethylcucurbit[5]uril as recoverable precatalysts for heck cross-coupling reactions[J]. Chem. Eur J., 2013, 19(46): 15661−15668.

[27] Zhao F, Wen B, Niu W H, Chen Z, Yan C, Selloni A, Tully C G, Yang X F, Koel B E. Increasing iridium oxide activity for the oxygen evolution reaction with hafnium modification[J]. J. Am. Chem. Soc., 2021, 143(38): 15616−15623.

[28] Yin J, Jin J, Lu M, Huang B L, Zhang H, Peng Y, Xi P X, Yan C H. Iridium single atoms coupling with oxygen vacancies boosts oxygen evolution reaction in acid media[J]. J. Am. Chem. Soc., 2020, 142(43): 18378−18386.

[29] You H H, Wu D S, Chen Z N, Sun F F, Zhang H, Chen Z H, Cao M N, Zhuang W, Cao R. Highly active and stable water splitting in acidic media using a bifunctional iridium/cucurbit[6]uril catalyst[J]. ACS Energy Lett., 2019, 4(6): 1301−1307.

[30] Cao M N, Wu D S, Gao S Y, Cao R. Platinum nanoparticles stabilized by cucurbit[6]uril with enhanced catalytic activity and excellent poisoning tolerance for methanol electrooxidation[J]. Chem. Eur J., 2012, 18(41): 12978−12985.

[31] Wu D S, Cao M N, Cao R. Replacing PVP by macrocycle cucurbit[6]uril to cap sub-5 nm Pd nanocubes as highly active and durable catalyst for ethanol electrooxidation[J]. Nano Res., 2019, 12(10): 2628−2633.

[32] Zhang S Y, Cao M N, Cao R. Multipod Pd-cucurbit[6]uril as an efficient bifunctional electrocatalyst for ethanol oxidation and oxygen reduction reactions[J]. ACS Sustain. Chem. Eng., 2020, 8(24): 9217−9225.

[33] Gong Z W, Wu D S, Cao M N, Zhao C, Cao R. Ultrafine Ru nanoclusters anchored on cucurbit[6]uril/rGO for efficient hydrogen evolution in a broad pH range[J]. Chem. Commun., 2020, 56(65): 9392−9395.

[34] Chen R R, Cao M N, Yang W G, Wang H M, Zhang S Y, Li H F, Cao R. Ultra-small Pd nanoparticles derived from a supramolecular assembly for enhanced electrochemical reduction of CO_2 to CO[J]. Chem. Commun., 2019, 55(66): 9805−9808.

[35] Song X M, Cao M N, Chen R R, Wang H M, Li H F, Cao R. Enhanced selectivity and stability towards CO_2 reduction of sub-5 nm Au NPs derived from supramolecular assembly[J]. Chem. Commun., 2021, 57(20): 2491−2494.

[36] Chen R R, Cao M N, Wang J Y, Li H F, Cao R. Decamethylcucurbit[5]uril based supramolecular assemblies as efficient electrocatalysts for the oxygen reduction reaction [J]. Chem. Commun., 2019, 55(78): 11687−11690.

[37] Khaligh A, Sheidaei Y, Tuncel D. Covalent organic framework constructed by clicking azido porphyrin with perpropargyloxy-cucurbit[6]uril for electrocatalytic hydrogen generation from water splitting[J]. ACS Appl. Energy Mater., 2021, 4(4): 3535−3543.

[38] Zhang C C, Liu X L, Liu Y P, Liu Y. Two-dimensional supramolecular nanoarchitectures of polypseudorotaxanes based on cucurbit[8]uril for highly efficient electrochemical nitrogen reduction[J]. Chem. Mater., 2020, 32(19): 8724−8732.

[39] Xie J, Peng H J, Huang J Q, Xu W T, Chen X, Zhang Q. A supramolecular capsule for reversible polysulfide stor-age/delivery in lithium-sulfur batteries[J]. Angew. Chem. Int. Ed., 2017, 56(51): 16223−16227.

[40] Xie J, Li B Q, Song Y W, Peng H J, Zhang Q. A supramolecular electrolyte for lithium-metal batteries[J]. Batteries Supercaps, 2020, 3(1): 47−51.

[41] Wang J, Ciucci F. *In-situ* synthesis of bimetallic phosphide with carbon tubes as an active electrocatalyst for oxygen evolution reaction[J]. Appl. Catal., B, 2019, 254: 292−299.

[42] Peng Q L, Chen J F, Ji H X, Morita A, Ye S. Origin of the overpotential for the oxygen evolution reaction on a well-defined graphene electrode probed by *in situ* sum frequency generation vibrational spectroscopy[J]. J. Am. Chem. Soc., 2018, 140(46): 15568−15571.

[43] Sun H M, Tian C Y, Fan G L, Qi J N, Liu Z T, Yan Z H, Cheng F Y, Chen J, Li C P, Du M. Boosting activity on Co_4N porous nanosheet by coupling CeO_2 for efficient electrochemical overall water splitting at high current densities[J]. Adv. Funct. Mater., 2020, 30(32): 1910596.
[44] Zhang X, Xu H M, Li X X, Li Y Y, Yang T B, Liang Y Y. Facile synthesis of nickel-iron/nanocarbon hybrids as advanced electrocatalysts for efficient water splitting[J]. ACS Catal., 2016, 6(2): 580−588.
[45] Wu D S, Cao M N, You H H, Zhao C, Cao R. N-doped holey carbon materials derived from a metal-free macrocycle cucurbit[6]uril assembly as an efficient electrocatalyst for the oxygen reduction reaction[J]. Chem. Commun., 2019, 55(92): 13832−13835.
[46] Xie J, Li B Q, Peng H J, Song Y W, Li J X, Zhang Z W, Zhang Q. From supramolecular species to self-templated porous carbon and metal-doped carbon for oxygen reduction reaction catalysts[J]. Angew. Chem. Int. Ed., 2019, 58(15): 4963−4967.
[47] Zhang S Y, Yang W G, Liang Y L, Yang X, Cao M N, Cao R. Template-free synthesis of non-noble metal single-atom electrocatalyst with N-doped holey carbon matrix for highly efficient oxygen reduction reaction in zinc-air batteries[J]. Appl. Catal., B, 2021, 285: 119780.
[48] Zhao H L, Yang S B, Yang W G, Zhao C, Cao M N, Cao R. Ultrasmall Mo_2C embedded in N-doped holey carbon for high-efficiency electrochemical oxygen reduction reaction [J]. Chemelectrochem, 2022, 9(10): e202200141.
[49] Xiao X, Zhang H, Xiong Y, Liang F, Yang Y W. Iridium-doped N-rich mesoporous carbon electrocatalyst with synthetic macrocycles as carbon source for hydrogen evolution reaction[J]. Adv. Funct. Mater., 2021, 31(42): 2105562.

瓜环基金属纳米催化剂的电化学研究进展

韦宗楠[a,b]，曹敏纳[b,*]，曹　荣[b,*]
[a] 中国科学技术大学化学与材料科学学院，安徽 合肥 230026
[b] 中国科学院福建物质结构研究所，福建 福州 350002

摘要

金属纳米材料在电催化应用中展示出良好的性能，但是它们依旧面临着稳定性差和调控策略有限的问题。引入第二组分是一种有效的策略，能够很好的改善其催化活性与稳定性。在这篇综述中，我们概述了结合金属纳米材料和瓜环（CB[*n*]）用于电催化应用。瓜环是一系列的具有刚性结构、高稳定性、与金属配位的官能团的大环，它们适合稳定金属纳米材料并对其进行调控。本文讨论按照瓜环的功能分类，包含瓜环作为保护剂、瓜环基的超分子自组装体以及瓜环作为前驱体制备氮掺杂多孔碳。多种金属纳米催化剂，包括金属纳米颗粒（Pt，Ir，Pd，Ru，Au）、金属单原子（Fe，Co，Ni）以及过渡金属碳化物（TMCs）成功与瓜环或瓜环衍生的碳材料复合，这些复合材料在许多电催化反应中展示出优异的性能和稳定性，反应包括了氧还原反应（ORR）、析氧反应（OER）、析氢反应（HER）、二氧化碳还原反应（CO_2RR）、甲烷氧化反应（MOR）、乙醇氧化反应（EOR）。其中，一些金属-瓜环复合物可进一步作为双功能催化剂用于全水解和燃料电池中。瓜环基的纳米催化剂具有媲美商用催化剂的性能，甚至其稳定性可优于商用催化剂。实验分析以及密度泛函理论（DFT）计算均证明了该提升得益于瓜环和金属纳米晶之间的相互作用以及瓜环自身的稳定性。最后，我们讨论了瓜环基电催化剂的挑战与机遇。本综述提供了通过瓜环构筑具有优异性能的金属纳米材料，并期待该策略将有助于开发高效催化剂并用于更多的电化学应用中。

关键词：电催化；燃料电池；电解水；瓜环；金属纳米材料